Macromolecules

pubs.acs.org/Macromolecules Article

Influence of Attractive Functional Groups on the Segmental Dynamics and Glass Transition in Associating Polymers

Ashesh Ghosh, Subarna Samanta, Sirui Ge, Alexei P. Sokolov,* and Kenneth S. Schweizer*

Cite This: https://doi.org/10.1021/acs.macromol.2c00080 Read Online

ACCESS | Metrics & More | Article Recommendations | Supporting Information

ABSTRACT: A recently developed microscopic statistical mechanical theory for how strong short-range attractions between sticky groups copolymerized in the backbone of associating polymer liquids perturb the segmental dynamics and glass transition temperature (T_g) is quantitatively compared with a large body of experimental data on end-functionalized telechelic melts of variable polymer backbone chemistry, association strengths, and chain lengths. For strong associations and PDMS-based telechelic melts, a universal growth in T_g is predicted and experimentally observed as a function of sticker fraction or telechelic chain length which does not depend on sticker chemistry. The predictions of a stronger than exponential growth of the alpha relaxation time, but perturbative or negligible changes in dynamic fragility, with increasing sticker fraction are also in good accord with the experimental observations. The theory is extended to the case of weaker sticker associations where the "transient cross-linked" network picture based on a large time scale separation between the nonsticker alpha relaxation time and the sticker bonding lifetime does not hold. The new physics is theoretically accounted for by introducing larger length scale dynamic sticker fluctuations consistent with weaker physical bonding. A smaller growth in T_g with sticker fraction is predicted which depends in a continuous manner on the degree of dynamical loosening of sticker bonding. The theoretical results are consistent with our experimental data for PPG-based telechelic melts. The theory provides guidelines for the design of polymers with dynamic bonds with controlled enhancements of T_g and segmental alpha time.

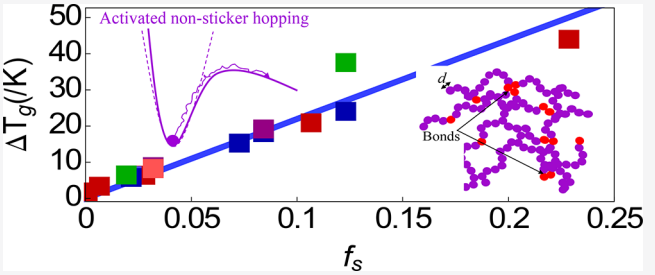

I. INTRODUCTION

Associating polymers with a relatively small fraction of "sticky" functionalities can exhibit strongly modified dynamical and rheological properties in semidilute solutions and melts. These systems are drawing increasing attention for applications as self-healing materials, biomaterials, rheological modifiers, sensors, and actuators.[1−12] Moreover, the polymers with "sticky" (dynamic) bonds provide easier recyclability.[13−15] The "sticky" groups (stickers) attract via variable strength chemistry specific interactions such as H-bonding, $\pi-\pi$ stacking, metal−ligand (M−L) interaction, ionic bond formation, and even dynamic covalent bonds (e.g., vitrimers).[16−20] Stickers can be arranged along the chain backbone at regular or random intervals, or at chain ends for telechelic systems, offering experimentally controllable sequence specific materials. The influence of sticky groups on polymer chain dynamics has been described theoretically at the coarse-grained level by using the so-called sticky Rouse and sticky reptation models,[21−27] and corrections were added in the refined bond lifetime renormalization model.[28] However, the presence of stickers can strongly alter the magnitude and temperature dependence of the primary alpha relaxation process in polymers,[17,28−35] which is not addressed in coarse-grained theories for chain dynamics and viscoelasticity. Sticker-induced modification of the alpha relaxation not only can result in a major shift of the glass transition temperature, T_g, but also affects the temperature and chemistry dependences of chain dynamics and rheological properties. Stickers affect the local dynamics of nonsticky segments in a manner that potentially depends on the melt density, sticker fraction, sticker monomer chemistry, and the specific backbone structure of the associating copolymer. Hence, a detailed microscopic understanding of how the stickers affect polymer segmental dynamics is a problem of high fundamental science and materials applications interest.

Two of us have recently formulated a microscopic, force-level statistical mechanical theory of the effect of stickers on the alpha relaxation time and glass transition temperature of nonstickers that goes beyond all existing phenomenological models.[36] However, to date, the new theoretical predictions have not been extensively compared with experimental observations. On the basis of a two-step dynamic framework

Received: January 12, 2022
Revised: February 21, 2022

https://doi.org/10.1021/acs.macromol.2c00080
Macromolecules XXXX, XXX, XXX−XXX

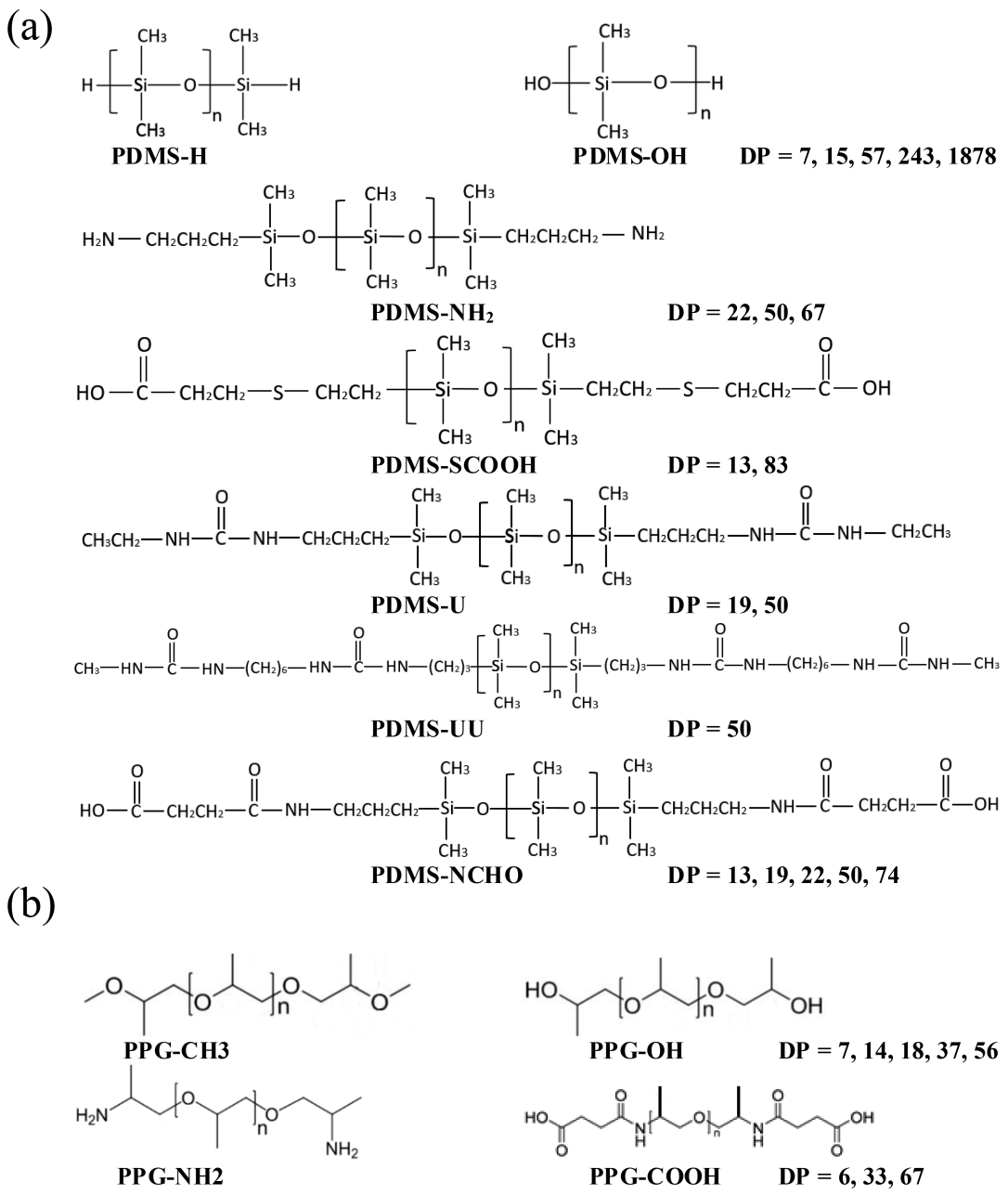

Figure 1. Telechelic (a) PDMS and (b) PPG with different end groups.

that involves the faster nonsticker alpha relaxation followed by a slower bond-breaking process,[37] the theory predicts the variation of the nonsticker alpha time, high-frequency elastic shear modulus, and change in T_g with sticker fraction.[36] In the strong attraction limit where the sticker lifetime significantly exceeds the nonsticker alpha time, our core hypothesis is that chemistry specific details, such as the precise nature of attraction, attraction strength (beyond a threshold), or even formation of clusters or microdomains and precise location of stickers along a polymer chain, are of secondary importance. The reason is we believe that the zeroth-order physics involves a transient cross-linked network-like picture where stickers are effectively immobilized or localized to small vibration-like motion *on* the time scale of the activated segmental alpha relaxation process. In essence, stickers serve as sites of immobility which enhance the kinetic constraints on the mobile nonstickers. If this simple physical picture is valid, the precise topology of sticker clustering is expected to be of secondary importance for the nonsticker alpha relaxation process. Rather, we propose that it is the concentration of stickers that is the leading order key variable that controls nonsticker alpha relaxation dynamics and changes of T_g, at least for the copolymer architectures studied here.

To test the detailed predictions of the theory and the above qualitative picture, this article presents *quantitative* comparisons with a large body of recent alpha relaxation time dielectric data for telechelic melts as a function of chain degree of polymerization (maps to the inverse degree of sticker functionalization) and sticker end group chemistry.[28−33] Beyond testing the theory for specific systems, we aim to explore whether a general behavior exists in the data as anticipated by our theoretical work. Our study is of fundamental polymer physics interest and also provides insights relevant to the design or selection of polymer

https://doi.org/10.1021/acs.macromol.2c00080
Macromolecules XXXX, XXX, XXX−XXX

chemistry variables to control the local dynamical properties, which in turn set the time scale for the longer length and time scale chain dynamics relevant to the viscoelasticity of associating copolymer materials. To address the special case of weak association relevant to some of the experimental systems considered, the theory is extended in the current article to go beyond the assumption in ref 36 that stickers act as literally fixed cross-links on the alpha relaxation time scale of the nonstickers. The extended theory retains the idea that the precise network topology is of secondary importance. However, it considers the possibility of weaker dynamic constraints on nonsticker-activated relaxation due to small scale sticker motion on times and length scales *well below* that characteristic of the sticker alpha relaxation time (α^* process). The sticker bond breaking time scale, and the question of larger time and length scale chain dynamics, are not addressed in our present work. However, we note that a theoretical framework for the relationship between the α and α^* processes has been recently proposed and quantitatively confronted with experiments on multiblock and telechelic associating polymer melts.[37]

Section II briefly describes the methods, synthesis, and measurement details of our experiments on the telechelic associating polymer melts, most of which has been previously discussed. Only the most important aspects of the microscopic theory developed in ref 36 are briefly summarized in section III, followed by its new extension to treat weakly associating copolymer liquids. In section IV we present the mapping procedure from an intermediate coarse-grained freely jointed chain (FJC) model to the polymer backbone chemistry of prime interest, poly(dimethylsiloxane) (PDMS). This calibrates the microscopic parameters from knowledge solely of the homopolymer reference melt behavior, thereby allowing us to make predictions for telechelics with *no* adjustable fit parameters. Sections V and VI present our predictions for the alpha relaxation time and T_g for the PDMS- and poly(propylene glycol) (PPG)-based telechelic melts, respectively, including quantitative comparisons with our experimental data.[28−33] The article concludes with a brief discussion and summary in section VII.

II. EXPERIMENTAL BACKGROUND

Methods and Synthesis. Chemical structures of the investigated PDMS and PPG samples are shown in Figures 1a and 1b, respectively. DP indicates the chain degree of polymerization, *n*. Of all the samples investigated in this study, PDMS-UU and PDMS-NCHO show a microphase-separated structure (cf. schematic in Figure 2) as evident in the SAXS data and two glass transitions.[38] The synthesis protocols of all the samples are given in the Supporting Information (section I).

Broadband Dielectric Spectroscopy. Broadband dielectric spectroscopy (BDS) in the frequency range 10^{-2}−10^{6} Hz was employed by using a Novocontrol system that includes an Alpha-A impedance analyzer and a Quatro Cryosystem temperature control unit. Most of the samples are liquid at room temperature (RT) and were placed in a parallel-plate dielectric cell made of sapphire and Invar steel with an electrode diameter of either of 12 or 10 mm. For the 12 mm electrode diameter system, a capacitance of 20 pF was obtained for the empty cell with an electrode separation of 49 μm. Empty cells with 10 mm electrodes and an electrode separation of 210 μm have a capacitance of 3.3 pF. PDMS-UU is a rubbery sample at room temperature (RT). Two gold-plated electrodes with a diameter of 20 mm were used to measure this sample; the separation between the electrodes was 174 μm. To avoid crystallization, most of the samples were initially quenched from RT to ∼113 K and reheated to 10 K below their respective glass transition temperature, T_g, prior to the measurements. After each temperature increase, the samples were equilibrated for at least 10−15 min to achieve thermal stabilization within 0.2K. More details of the experimental procedures for each of the investigated samples can be found elsewhere.[28−33,38]

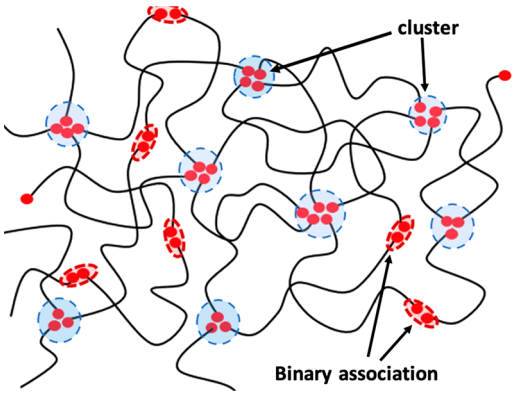

Figure 2. Cartoon of the phase-separated structures in the melt state of the associating telechelic polymers. The stickers are represented as red spheres, and polymer chains are shown as black curves. Stickers can associate with each other via binary interactions (maroon ellipses) or form phase-separated clusters (blue circles) due to their immiscibility with the polymer matrix. Out of all the systems studied here, only PDMS-UU and PDMS-NCHO showed microphase-separated domains.

T_g and Association Activation Energy Estimation. BDS measures the segmental relaxation (alpha process) of the polymer and additionally chain relaxation in the case of PPG.[29] The association−dissociation process of stickers changes the overall dipole moment of the system and appears as an additional dielectric signal with a characteristic time scale given by the association/dissociation lifetime of the end groups.[29] Here we refer to this signal as the α^* process. Dielectric spectroscopy provides direct measurements of the time scales of these two processes and can provide rough estimates of the apparent activation energy (E_a) of the sticker dissociation defined via the Arrhenius equation:[21,31,37,39−42]

$$\tau_{\alpha^*}(T) = \tau_{\alpha}(T)\exp\left(\frac{E_a}{RT}\right) \quad (1)$$

The activation energy varies strongly with molecular structure of the end groups (Figure 3). While the Arrhenius equation (eq 1) does not address the two-step nature of the α^* process involving α-relaxation followed by bond breaking,[37] and hence fails in some cases,[31,37] it

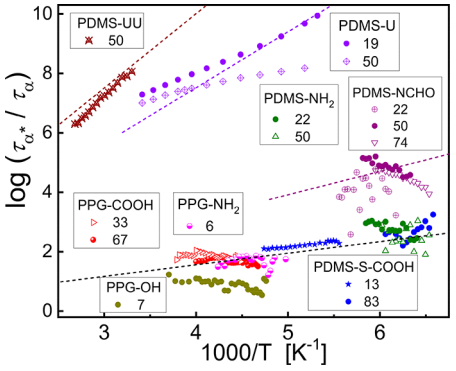

Figure 3. Logarithm of the ratio of the sticker dissociation and segmental relaxation time scales vs inverse temperature for the investigated telechelic polymers. The straight lines correspond to activation energies of 48, 36, 15, and 7.5 kJ/mol (top to bottom) per eq 1. A higher slope indicates a higher activation energy of the dissociation process.

https://doi.org/10.1021/acs.macromol.2c00080
Macromolecules XXXX, XXX, XXX−XXX

provides a good zeroth-order estimate of the chemistry-specific bond-breaking energy. Extrapolation of the segmental relaxation time to $\tau_\alpha \sim 100$ s using the Vogel–Fulcher–Tamman (VFT) equation, $\tau_\alpha(T) = \tau_0 \exp\left(\frac{B}{T - T_0}\right)$,[29−31] provides an estimate of T_g where the parameters of limiting relaxation time (τ_0), B, and VFT temperature T_0 for all the systems are given in refs 28 and 29. The estimated T_g and E_a for the telechelic polymers studied here are presented in Tables 1 and 2 for the PDMS and PPG systems, respectively. While the activation energies of all PDMS telechelic systems and PPG-COOH are relatively high, that of PPG-OH is low. This indicates two distinct cases where $\tau_{\alpha^*} \gg \tau_\alpha$ (PDMS, strong bonds ≡ large time scale separation) and $\tau_{\alpha^*} \gtrsim \tau_\alpha$ (PPG, relatively weaker bonds ≡ small/modest time scale separation). Additionally, we show the difference in T_g, defined as ΔT_g, estimated as the difference between T_g of the polymer with associating functional end groups and T_g of the polymer with the *same* DP but with nonassociating chain ends (−H or $-CH_3$).

Table 1. Total Molecular Weight and Degree of Polymerization-Dependent Dielectric T_g (BDS), Change in Glass Transition Temperature Compared to the Reference Nonassociating Polymer, and Activation Energy Determined from Eq 1 for PDMS Telechelic Associating Polymers

polymer	M_n (g/mol)	DP	T_g (K)	ΔT_g (K)	E_a (kJ/mol)
PDMS-OH	400−700	7	170	38	
	700−1500	15	154	15.5	
	4200	57	146	3.5	
	18000	243	145	1.5	
	139000	1878	144	0	
PDMS-NH_2	1738	22	151	11	9.1 ± 0.2
	3816	50	147.5	5	7.6 ± 0.3
	5592	67	146.5	3.5	8.3 ± 0.2
PDMS-SCOOH	1228	13	169.5	32	8.2 ± 0.4
	6408	83	147	4	8.1 ± 0.2
PDMS-U		19	154	14	37.3 ± 0.5
		50	148	5.5	33 ± 0.8
PDMS-NCHO	1280	13	156	18.5	19.9 ± 0.2
	1720	19	153	13	16.7 ± 0.4
	1940	22	151	11	13.5 ± 0.4
	4020	50	148	5.5	15.4 ± 0.3
	5570	74	146	3	13.7 ± 0.4
PDMS-UU		50	147.5	5	46 ± 0.2

Table 2. Molecular Weight and Degree of Polymerization-Dependent Dielectric T_g (BDS), Change in Glass Transition Temperature from Reference Nonassociating Polymer, and Activation Energy Determined from Eq 1 for PPG Telechelic Associating Polymer

polymer	M_n (g/mol)	DP	T_g (K)	ΔT_g (K)	E_a (kJ/mol)
PPG-CH_3	468	7	172		
	874	14	183		
	1106	18	185.5		
	2208	37	194.5		
	3310	56	194.5		
PPG-OH	440	7	196	24	3.9 ± 0.2
	846	14	198	15	
	1078	18	200	14.5	
	2180	37	201	6.5	
	3282	56	201	6.5	
PPG-NH_2	480	6	192.5	24.5	5.8 ± 0.1
	2046	33	199	6.5	
	4018	67	200	5.5	
PPG-COOH	680	6	248	80	8.4 ± 0.2
	2246	33	213.5	21	8.5 ± 0.1
	4218	67	205.5	11	7.3 ± 0.1

III. THEORETICAL BACKGROUND

Our recently developed statistical mechanical theory to predict activated segmental relaxation and vitrification of associating regular AB multiblock copolymer melts (single sticker sites separated by a fixed number of nonstickers) has been discussed in detail in ref 36. Successful confrontation with alpha time data for randomly functionalized multiblock ionomer materials was also presented. Here we briefly sketch the crucial aspects of the prior theory and model employed.

Model and Large Time Scale Separation Limit. Previous work considered a liquid of regular copolymers composed of chains of N connected sites all of the same diameter d with single associating sites or "stickers" placed along the backbone at regular intervals with a fraction denoted by f_s (Figure 4A). A freely jointed-chain (FJC) model with persistence length $l_p/d = 4/3$ was utilized, and the modest self-overlap of interaction sites of such an ideal chain model is considered[43] to define an effective space-filling melt packing fraction, ϕ_{eff}. All sites on different chains interact via the same hard-core repulsion. Stickers attract via an exponential pair potential beyond hard-core contact with a variable contact strength ($\beta\epsilon$ in thermal energy units) of a short spatial range of $a/d = 0.10$ characteristic of a specific attraction.

Per Figure 4B, the three interchain site–site pair correlation functions, $g_{\alpha\beta}(r)$, their analogous partial collective static structure factors in Fourier space, $S_{\alpha\beta}(q)$, and the corresponding site–site direct correlation functions, $C_{\alpha\beta}(q)$, are computed by using the Polymer Reference Interaction Site Model (PRISM) integral equation theory[44−46] with the Percus–Yevick (PY) closure.[44−47] See ref 36 and references therein for all technical details. Our prime focus previously was the high-attraction regime where effectively all stickers are bonded to other stickers.

The formal starting point to treat activated dynamics based on the Elastically Collective Nonlinear Langevin Equation (ECNLE) theory[48,49] is to relate the strength of kinetic constraints that enter calculation of the force–force time correlation function associated with any tagged segment to the equilibrium interchain site–site pair correlation functions. The force correlations on a nonsticker segment have multiple origins or dynamic pathways,[36,50] as schematically shown in Figure 5. The effective force on a segment consists of an effective intermolecular pair repulsion between all sites and an attractive bonding force between stickers that is explicitly treated based on the recently developed (and extensively applied to attractive colloid suspensions) Projectionless Dynamic Theory (PDT).[51,52] Our focus is on the activated hopping of nonstickers when there is sufficient time scale separation that the slower stickers form physical bonds modeled in a localized harmonic or Gaussian manner (not literal pinning), the vibrational amplitude of which is a priori predicted from the naïve mode coupling theory (NMCT) self-consistent localization equations.[36] The ideas are schematically shown in Figure 4C.

https://doi.org/10.1021/acs.macromol.2c00080
Macromolecules XXXX, XXX, XXX−XXX

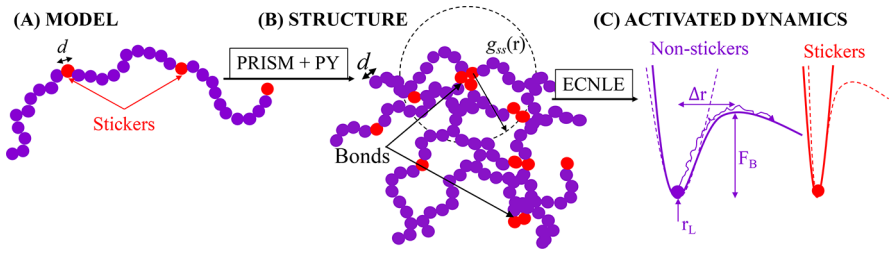

Figure 4. Schematic of the key elements of the associating copolymer theory.[36] (A) Regularly spaced sticker copolymer chain model. Red and purple beads represent stickers and nonstickers, respectively. (B) PRISM integral equation theory is used to obtain intermolecular site−site pair correlations functions. (C) Knowledge of (B) is input to quantify dynamic constraints and construct the dynamic free energies in the ECNLE theory of activated relaxation. Crucial local length and energy scales are the transient localization length (r_L), cage barrier height (F_B), and jump distance (Δr).

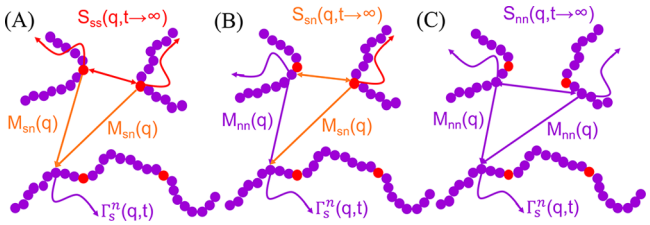

Figure 5. Schematic of interchain force−force time correlation pathways for nonsticky segment self-motion for a copolymer chain having sticky (red) and nonsticky (purple) groups. Force−time correlations decay in time in a parallel manner due to tagged nonsticker segment motion encoded in its dynamic self-correlation function, , $\Gamma_s^n(q, t)$, and the collective motion of the copolymer liquid. Beyond the NMCT onset where segments first become transiently localized, the latter enters the NLE theory construction of the dynamic free energy via site-specific collective Debye−Waller factors, $S_{ij}(q,t \to \infty)$, where $(i, j) \in (s, n)$. The corresponding single particle (incoherent) dynamic structure factor becomes a Gaussian Debye−Waller (DW) factor as $\Gamma_s^n(q, t \to \infty) = \exp(-q^2 {r_L}^2/6)$, corresponding to the localized form of $\Gamma_s^n(q, t) = \exp(-q^2 r_n(t)^2/6)$.

The scalar displacement of a tagged nonsticker segment, $r_n(t)$, obeys a stochastic nonlinear Langevin equation (NLE),[36,50]

$$\zeta_{s,n}\frac{\mathrm{d}}{\mathrm{d}t}r_n(t) - \frac{\partial F_{\mathrm{dyn}}(r_L^s, r_n(t))}{\partial r_n(t)} + \delta f_n(t) = 0 \tag{2}$$

where $\zeta_{s,n}$ is the nonsticker short time friction constant, $\delta f_n(t)$ is the corresponding random fluctuating force that obeys $\langle \delta f_n(0)\ \delta f_n(t)\rangle = 2k_B T\zeta_{s,n}\delta(t)$, and $F_{\mathrm{dyn}}(r_L^s, r_n(t))$ is the nonsticker dynamic free energy that is a function of a tagged-segment instantaneous displacement *and* parametrically depends on the predicted ensemble-averaged sticker localization length, r_L^s. In the overdamped dynamical regime of interest, a short time nonactivated process enters with a characteristic time scale $\tau_s = \beta\zeta_{s,n}\sigma^2$ that is explicitly given by[48]

$$\frac{\tau_{s,n}}{\tau_0} = 1 + \frac{1}{36\pi\varphi_{\mathrm{eff}}}\int_0^\infty \mathrm{d}q\ \frac{q^2(S_{nn}(q) - 1)^2}{S_{nn}(q) + (1 - j_0(q) + 2j_2(q))^{-1}} \tag{3}$$

Here, $j_n(x)$ is the spherical Bessel function of order n, and τ_0 is a "bare" time scale written in a manner akin to a hard-sphere fluid as $\tau_0 = \frac{g_{nn}(d)}{24\rho d^2}\sqrt{\frac{M}{\pi k_B T}}$, where $g_{nn}(d)$ is the contact value of the interchain site−site pair correlation function, $g_{nn}(r)$. This short time scale only enters as a prefactor in the alpha relaxation hopping time and does not change with sticker fraction. Although chain connectivity is considered when computing structural correlations with PRISM theory which enter the so-called dynamic force vertex (see below), it is ignored for the dynamic hopping event.[36] This simplification has been discussed in detail in ref 36. It is physically reasonable since the jump distance is predicted to be small compared to the polymer persistence length and bead diameter.

The nonsticker dynamic free energy is explicitly given by (see ref 36 for all details)

$$\begin{aligned} F_{\mathrm{dyn}}(r_L^s, r_n) - F_{\mathrm{dyn}}(r_L^s, r_L^n) &= \int_{r_{L,n}}^{r_n}\frac{\partial F_{\mathrm{dyn}}(r_L^s, r_n)}{\partial r_n}\,\mathrm{d}r_n \\ &= -3\ln\left(\frac{r_n}{r_L^n}\right) + \frac{1}{18\pi^2}\int_{r_{L,n}}^{r_n}\mathrm{d}r_n'\,r_n' \\ &\int_0^\infty \frac{\mathrm{d}q}{(2\pi)^3}q^2 \mathrm{e}^{-q^2 r_n'^2/6}[M_{nn}(q)^2 S_{nn}(q, t\to\infty) \\ &+ M_{sn}(q)^2 S_{ss}(q, t\to\infty) + M_{nn}(q) \\ &M_{sn}(q)\{S_{sn}(q, t\to\infty) + S_{ns}(q, t\to\infty)\}] \end{aligned} \tag{4}$$

It considers dynamic constraints due to several types of interchain forces as schematically shown in Figure 5. The effective force vertices $M_{\alpha\beta}(q)$ are written in terms of the site−site direct correlation function in Fourier space for hard-core repulsive interactions, while attractive interactions are treated explicitly based on the hybrid projectionless dynamic theory (hybrid-PDT); see refs 36 and 51 for all details. The quantities $S_{\alpha\beta}(q,t \to \infty)$ are the long time arrested (at the naive mode coupling theory (NMCT) level) quantities which enter NLE theory for the dynamic free energy as collective dynamic structure factors. The latter are essentially Debye−Waller factors and depend on the sticker localization length r_L^s; e.g., for a one-component liquid $S(q, t \to \infty) = \exp\left[-\frac{q^2 {r_L}^2}{6S(q)}\right]$. As before, we assume sticker relaxation and bond breaking is slow (the α^*-process) compared to nonsticker relaxation, corresponding to a two-step dynamical relaxation scenario.[37] On the nonsticker relaxation time scale of interest, the stickers effectively only vibrate on very small length scales around their predicted localization length in the spirit of a "transient network" (solid red curve in Figure 4C). Such highly restricted local sticker motion is physically expected, and assumed in our analysis, to be independent (to leading order) of the precise

https://doi.org/10.1021/acs.macromol.2c00080
Macromolecules XXXX, XXX, XXX−XXX

copolymer architecture, e.g., multiblock vs telechelic. An example dynamic free energy is schematically shown in Figure 4C (solid blue curve).

The defining feature of ECNLE theory is the idea that the cage scale barrier hopping event controlled by the dynamic free energy generically requires the polymer segments beyond the cage scale to dynamically displace by a small amount in a long-range collective elastic manner. This contributes an additional elastic barrier which has been derived to be[36]

$$\beta F_e^n = 12\varphi_{\rm eff}^n (\Delta r_{\rm eff}^n)^2 \left(\frac{r_{\rm cage}}{\sigma}\right)^3 K_0^n \quad (5)$$

where $\varphi_{\rm eff}^n = (1 - f_s)\varphi_{\rm eff}$. The *effective* jump distance associated with a segment leaving its cage sets the amplitude of the collective elastic displacement field and enters the elastic barrier quadratically. It is explicitly given by $\Delta r_{\rm eff}^n = \frac{3}{32}\frac{(r_B^n - r_L^n)^2}{r_{\rm cage}}$, where r_B^n is the location of nonsticker dynamic free energy barrier and K_0^n is the harmonic spring constant of the minimum (localized state) of the dynamic free energy given as $K_0^n = \frac{3k_BT}{(r_L^n)^2}$, with the cage radius $r_{\rm cage} = 1.5d$.

When the local cage barrier is larger than ∼1−2 thermal energy units, the mean nonsticker alpha time is given by the simplified form of Kramers theory as

$$\frac{\tau_\alpha}{\tau_s} = 1 + \frac{2\pi}{\sqrt{K_0^n \times K_B^n}} \exp(\beta(F_B^n + F_e^n)) \quad (6)$$

where K_B^n is the absolute value of the harmonic curvature of the dynamic free energy maximum at the barrier location.

Beyond the Large Time Scale Separation Limit: Larger Sticker Fluctuation. In the theory discussed so far, when constructing the nonsticker dynamic free energy the stickers are modeled as fluctuating (or vibrating) in a Gaussian manner around their predicted dynamic localization lengths (see Figure 4C). This "vibrational pinning" representation of a physical bond implies the stickers remain fully bonded on the time scale of the nonsticker alpha relaxation and mimics a transient rubber network like state. For weak enough associations this approximation must eventually fail. One can imagine stickers "dynamically moving" along their own free energy curve in the direction of larger displacements (ala a fast beta process or early stage alpha process) due to thermal fluctuations on the time scale of the nonsticker alpha relaxation.[36] Whether this is important or not for nonsticker dynamics is expected to be nonuniversal and polymer chemistry (e.g., association bond strength) dependent. Within our simplified framework this physics is crudely mimicked by allowing the sticker dynamic fluctuations to be larger than their strictly predicted localization length (at the minimum of the corresponding dynamic free energy), thereby weakening their dynamical constraints on nonsticker activated motion. Our basic physical picture is retained, and the larger sticker displacements (but still small compared to the nonsticker displacements characteristic of the alpha process) result in weaker dynamic constraints on nonsticker activated relaxation.

Figure 6A shows a schematic of this idea and how we implement it. Representative consequences for the nonsticker dynamic free energy at a packing fraction $\phi_{\rm eff} = 0.58$ (where the homopolymer relaxation time is ∼1 ns using $\tau_0 = 1$ ps) and fixed sticker fraction $f_s = 0.1$ are shown in Figure 6B. As the sticker effective localization length increases ($r_L^{s\prime} > r_L^s$), dynamic constraints on the nonstickers decrease, resulting in a large nonsticker localization length (minimum of its dynamic free energy, r_L^n), a lower cage barrier, F_B^n, and a smaller elastic barrier. For $r_L^{s\prime} = r_L^s + 0.33\Delta r_n$, where $\Delta r_n = r_B^n - r_L^n$ is the nonsticker jump distance which is a function of f_s, the cage barrier is similar to that of pure homopolymer melt for $f_s \leq 0.10$.[53] The collective elastic barrier and mean hopping time from Kramers theory can be calculated as before,[36] which then yields the nonsticker alpha relaxation time.

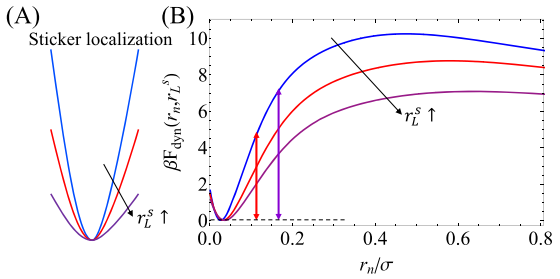

Figure 6. (A) Schematic of the weakened physical bonding constraint model where stickers are allowed to fluctuate in a Gaussian manner with a larger localization length than a priori predicted by using NMCT. (B) Representative example of the consequences of (A) for the nonsticker dynamic free energy at a fixed copolymer melt packing fraction of $\phi = 0.58$ and $f_s = 0.10$. Blue, red, and purple colors indicate sticker localization lengths of $r_L^{s\prime} = r_L^s$, $r_L^s + 0.25\Delta r_n$, and $r_L^s + 0.33\Delta r_n$, respectively, all of which are well below the barrier and hence correspond to late beta or early alpha time dynamic fluctuations. The locations of $r_L^s + 0.25\Delta r_n$ and $r_L^s + 0.33\Delta r_n$ on the homopolymer dynamic free energy are shown by vertical colored arrows. At $r_L^{s\prime} = r_L^s + 0.33\Delta r_n$, the local cage barrier is nearly the same as if no stickers were present, per a nonassociated homopolymer melt.

IV. NONSTICKER ALPHA TIME: MODEL CALCULATIONS AND PDMS HOMOPOLYMER MELTS

Basic Results for Associating Copolymer Melts. As relevant background, theoretical results for the nonsticker mean alpha time of the AB associating copolymer melt model are shown in Figure 7 as a function of effective liquid packing fraction for various sticker fractions and $\tau_0 = 10^{-12}$ s. The alpha time grows supraexponentially with increasing melt packing fraction and sticker concentration. For example, for $\phi_{\rm eff} = 0.56$ a sticker fraction of $f_s = 10\%$ increases the alpha time by ∼2

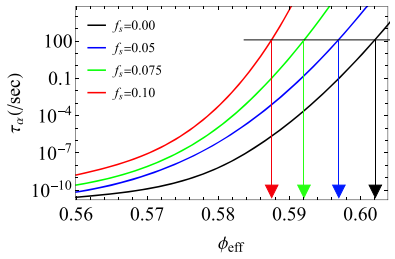

Figure 7. Alpha relaxation time (in seconds) as a function of effective packing fraction for various sticker fractions. The elementary time scale is taken as $\tau_0 = 1$ ps. The horizontal black line defines an experimentally relevant kinetic vitrification transition corresponding to $\tau_\alpha(\phi_g) = 100$ s. Vertical colored lines correspond to different $\phi_g(f_s)$ values.

https://doi.org/10.1021/acs.macromol.2c00080
Macromolecules XXXX, XXX, XXX−XXX

decades, while for a higher $\phi_{\text{eff}} = 0.585$ the same sticker fraction increases the alpha time by ∼7 decades. Such a large difference reflects the growing absolute and relative (to the local cage barrier) importance of collective elasticity.

We define an operational laboratory glass transition temperature as when $\tau_\alpha = 100$ s, which corresponds to $\phi_{\text{eff}} \approx 0.60$ for the homopolymer melt ($f_s = 0$). This isochronal vitrification criterion is the horizontal black line in Figure 7. A shift in the glass transition melt packing fraction in associating copolymers, $\Delta\phi_g = \phi_g(f_s) - \phi_g(0) \leq 0$, is indicated by the vertical lines in Figure 7 and implies increased dynamic caging constraints experienced by nonstickers due to the presence of more localized sticker segments.

Temperature Mapping and Calibration to PDMS Homopolymer Melt. To relate the alpha time results in Figure 7 to a specific chemistry and temperature under 1 atm isobaric conditions, we adopt the well-known dimensionless compressibility (S_0) mapping that employs the experimental polymer liquid equation of state (EOS),[54]

$$S_{0,PY}^{\text{homopolymer}}(\varphi_{\text{eff}}) \equiv S_{0,\text{expt}} = \rho k_B T \kappa_T \approx N_s^{-1}\left(-A + \frac{B}{T}\right)^{-2} \tag{7a}$$

$$T(\phi_{\text{eff}}) = \frac{B}{A + \frac{1}{\sqrt{N_s S_{0,PY}^{\text{homopolymer}}(\phi_{\text{eff}})}}} \tag{7b}$$

where the final approximate equality in eq 7a is a good analytic approximation. The parameters A and B are related to entropic and enthalpic contributions in the EOS, respectively, and N_s quantifies how many elementary functional groups a bead or segment in the FJC model represents. These parameters can be estimated from experimental data, which then provides a *polymer-specific* mapping from effective packing fraction to temperature. It has been previously shown that adopting either the numerical S_0 value computed from PRISM−PY integral equation theory of a connected polymer chain melt, or a literal mapping to a disconnected hard-sphere (HS) liquid of Kuhn segments by using $S_{0,PY}^{HS} = \frac{(1-\phi)^4}{(1+2\phi)^2}$, yields very similar results for the mapping and predicted dynamics.[36] We use the former approach, which results in eq 7b.

In practice, the purely end-functionalized telechelic melt systems of present interest exhibit a degree of polymerization (DP)-dependent glass transition temperature.[28−33] Because the DP is inversely proportional to the fraction of end groups, we write $f = a/DP$, where a is a proportionality constant. In principle, its precise value is related to the level of coarse graining employed in the theory model (i.e., what a model bead corresponds to in terms of real chemical monomers) and hence the detailed polymer chemistry. One can view a as a polymer-specific adjustable parameter in our theoretical analysis. However, we have attempted to realistically estimate it using homopolymer PDMS parameters[54] and find $a \approx \frac{C_N}{N_s} \sim 1.6$ using a PDMS characteristic ratio (C_N) of ∼6.3, and N_s is the number of elementary functional groups in a lightly coarse-grained bead which we find to be close to ∼4.

To focus on the effects of physical bonding of associating end groups on the change of the glass transition temperature, we calibrate $N_s(f)$ (here f is inversely related to the homopolymer degree of polymerization, N) to ensure the theory and model reproduce the experimental reference f-dependent PDMS *homopolymer* glass transition temperature, $T_g(f)$, and fragility, $m(f)$, in the *absence* of associating end groups. The experimental PDMS homopolymer melt glass transition temperature and fragility values[54] employed for this calibration are given in the Supporting Information (section II). From PDMS EOS data[54] it is known that $A = 0.675$ and $B = 1057$ K in eqs 7a and 7b which are employed for all end group fractions f. We then fix $\tau_0 = 10^{-12}$ s and vary N_s to reproduce T_g and m for each variable DP homopolymer melt of interest with an end group fraction, f. As discussed in the SM, a modest variation of $N_s \sim 4.3$ to ∼3.5 changes T_g from ∼144 K at $f \sim 0$ (long chain limiting behavior) to ∼130 K at $f \sim 0.20$.

Figure 8 shows a typical result for the temperature-dependent homopolymer alpha relaxation time in the deeply supercooled regime and the limiting long chain behavior where T_g and fragility become independent of DP. Also shown in the inset is the corresponding $\phi_{\text{eff}} - T$ mapping obtained by using eq 7b. Because we only calibrate the model parameters with respect to the $\tau_\alpha = 100$ s state (for both T_g and m), the theoretical results in Figure 8 represent *predictions* for all temperatures above T_g. At high enough temperatures deviations are found, as expected based on using a coarse-grained model, but overall, the theory agrees well with experiment in the *deeply* supercooled regime close to kinetic vitrification which is of prime interest in this work.

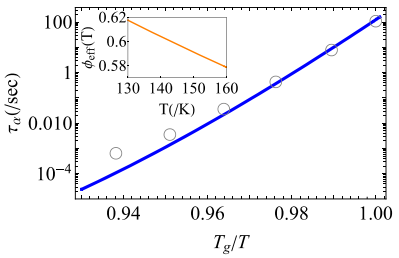

Figure 8. Theoretical prediction for the alpha relaxation time compared to experiment for the long chain limit of the PDMS homopolymer melt studied in ref 54. The theory based on the coarse-grained FJC model deviates from experimental results at high temperature (as expected), and hence in this work we focus on the deeply supercooled regime relatively close to T_g. The inset shows the mapping from effective packing fraction to temperature for PDMS.

Once we have calibrated the model to account for the f-dependent homopolymer melt T_g and fragility behavior, the theory can be used to make *no* adjustable parameter predictions for associating copolymer melts based on assuming that the telechelic EOS is the same as for pure PDMS. The latter approach is adopted both for simplicity and to allow predictability given the lack of associating copolymer experimental EOS data to "precisely" carry out the mapping for each telechelic individually.

V. APPLICATION TO PDMS-BASED TELECHELIC MELTS

Shift in T_g. The DP and sticker fraction dependent change in glass transition temperature is

$$\Delta T_g = T_g(f_s = f) - T_g(f) = \{T_g(f \to \infty) - T_g(f)\} + \{T_g(f_s = f) - T_g(f \to \infty)\} \tag{8}$$

https://doi.org/10.1021/acs.macromol.2c00080
Macromolecules XXXX, XXX, XXX−XXX

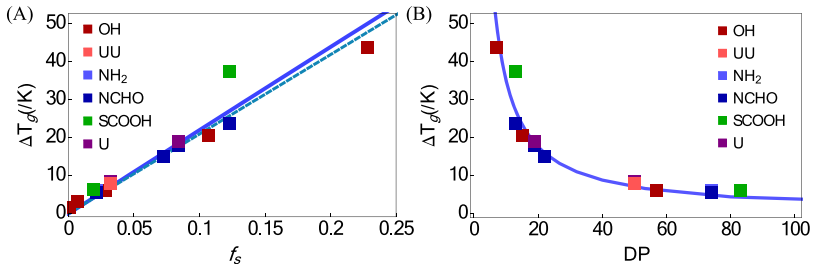

Figure 9. (A) Change of T_g compared to the DP-dependent homopolymer melt as a function of sticker fraction for various sticker chemical moieties attached to a PDMS backbone. Different end groups are color-coded by different squares as indicated. The a priori theoretical prediction (not a fit, no adjustable parameters) is the solid blue curve. The dashed blue curve is an empirical linear fit through all the experimental points and follows the predicted theory curve very closely. (B) The plot shows the same change in T_g as a function of DP where DP = 1.60/f. The blue curve is the theoretical prediction.

where the reference $T_g(f)$ in eq 8 corresponds to the DP-dependent homopolymer glass transition temperature. The contribution $T_g(f \to \infty) - T_g(f)$ reflects changes in dynamical constraints due to nonassociating homopolymer chain length and always contributes positively; i.e., T_g grows and then saturates with degree of polymerization. The term $T_g(f_s = f) - T_g(f \to \infty)$ captures the changes due to the enhanced dynamical constraints in an associating polymer due to physical bonding of stickers relative to the DP $\to \infty$ limit (highest T_g of a homopolymer). It can in principle be positive (strongly associating systems), close to zero (moderately associating systems), or even negative (repelling or weakly associating end groups). For PDMS, both contributions are positive and increase the glass transition temperature. However, we will also discuss a PPG telechelic in section VI where the second contribution in eq 8 can be positive or negative depending on the precise nature of the associating end group. Of course, dynamic caging constraints experienced by nonstickers will always increase with sticker concentration, resulting in an increase of the copolymer T_g.

Theoretical predictions for PDMS telechelic melts as a function of sticker fraction are shown in Figure 9A. Numerically, for f_s = 0.1 one sees T_g changes by ∼20 K, while at f_s = 0.20, T_g is larger by ∼40 K. Remarkably, we find the growth in T_g follows an almost perfect *linear trend* with sticker fraction. This is not a trivial "chain end" approach as in phenomenological free volume models (e.g., Flory–Fox[56,57]); indeed, those models attempt to mimic the *decrease* of T_g as chain length decreases, the opposite direction of T_g changes in the associating systems.

To compare the theoretical results with experiment, we convert telechelic degree of polymerization (DP or n) to sticker fraction, f_s. Because, as discussed above, DP is inversely related to sticker fraction, one has $f_s = a/DP$ where $a \approx 1.6$. All our analysis below uses this conversion between theoretical sticker fraction and experimental DP.

Figure 9A plots the experimental change in T_g as a function of sticker fraction for six choices of sticky end group (see data in Table 1) which have variable strengths of attraction between stickers as well as some degree of microphase separation for PDMS-NCHO and PDMS-UU. Overall, we find remarkably good agreement with theory, especially given this is *not* a fit, and no adjustable parameters have been introduced. This agreement for the telechelic melts considered is consistent with the assumed sufficiently large time scale separation between the α and α^* processes adopted in the theoretical analysis where the precise nature of attractive functionality does not matter to zeroth order. It is also consistent with our physical idea that higher scale structuring (clusters, microphase separation) is not important to leading order for the questions of interest. A linear fit of all the experimental data points is also shown, which agrees almost perfectly with theory. The same results are plotted as of T_g vs DP in Figure 9B showing the same degree of agreement, where the theoretical f_s is converted to DP by using DP = 1.60/f_s.

Alpha Relaxation Time: Temperature and Sticker Fraction Dependences. We quantitatively confront theory and PDMS-NCHO-COOH melt experiments for the alpha time as a function of inverse temperature (normalized by T_g) in Figure 10. VFT fits of the experimental data points are shown as dashed curves, while theory predictions are the solid curves. The level of theory–experiment agreement for the full temperature dependence of the alpha time is reasonable for all sticker fractions studied experimentally which range from f_s = 0.028–0.124.

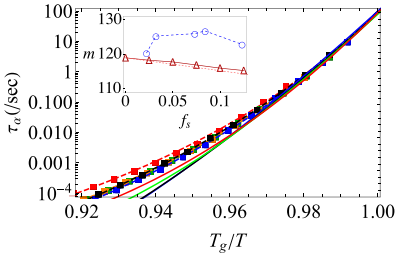

Figure 10. Angell plot of the experimental alpha time data and theory predictions for sticker fractions of 0, 0.05, 0.075, and 0.10 (solid curves are theory, from blue to red, bottom to top) and 0.022, 0.032, 0.073, 0.084, 0.123 (experiment, points). Dashed curves are VFT fits through the experimental points. Inset shows the fragility of the experimental PDMS-NCHO systems (blue circles) obtained from the VFT fits and the corresponding theoretical predictions (red).

Results for the dynamic fragility, $m = \frac{\mathrm{d}\log\tau_\alpha}{\mathrm{d}(T_g/T)}$ at $T = T_g$, are shown in the inset. Globally, and nontrivially, it is nearly constant to leading order. The theory predicts a perturbative but systematic decrease in the fragility with increasing sticker fraction. As expected, the overall agreement between theory and experiment for fragility is good but not perfect. More generally, given all the simplifications made in the modeling, and the fact that fragility is a subtle feature since it is the ratio of an inverse temperature derivative quantity to T_g, the level of agreement seems reasonable. The prediction of a small 4% decrease in fragility with sticker fraction versus roughly constant fragility observed in experiment could be due to

https://doi.org/10.1021/acs.macromol.2c00080
Macromolecules XXXX, XXX, XXX–XXX

many hard to disentangle factors such as (i) the theory employs an associating multiblock polymer model while experiments are performed on telechelics, some of which show microphase separation, (ii) a coarse-grained FJC model is employed that ignores the chemistry of the real end groups and PDMS monomers, (iii) the experimental equation of state (EOS) is presumably weakly sticker fraction dependent factor which is ignored, (iv) in reality there is not an infinite separation of time scales between the α and α^* process but we assume there is in our adopted strict two-step dynamic scenario, and (v) other chemical effects such as possible backbone stretching, changes of C_N with telechelic DP, and so on. Remarkably, all these effects apparently have very small consequences, indicating a high degree of "self-averaging" of subnanometer scale chemical structure for the dynamical properties we study.

We note that although deviations of the experimental results from the theory predictions are found at higher temperatures (smaller T_g/T values), they are qualitatively identical with those present for the reference pure homopolymer PDMS melt discussed in section IV. Thus, we believe that these deviations relate primarily to the coarse-grained model adopted, although the other second order factors (i−v) mentioned above could also contribute. More crucially, as one transitions from a low to high sticker fraction, the deviations are similar in magnitude as seen in Figure 10 (cf. blue vs red plots at fixed T_g/T values). Hence, to zeroth order, the observed deviations do not depend on sticker fraction or the physics of bond formation.

Theory and experiment are further confronted in Figure 11 for the alpha time as a function of sticker fraction at several fixed reduced temperatures, $\frac{T}{T_g}$, where T_g is the DP-dependent glass transition temperature of the homopolymer melt. Experimental points are shown as filled squares, with the τ_α > 10 s points obtained from extrapolated VFT fits to the experimental data at temperatures close to the glass transition for the PDMS-NCHO samples.[58] Overall, there is very good accord between theory (*no fitting* parameter) and experiment for all trends, and the agreement is (remarkably) almost quantitative. In detail, at the lowest sticker fraction studied in the experiments (f_s = 0.022), as $\frac{T}{T_g}$ changes from 1.20 to 1.08, the alpha time increases by ∼4 decades, while at f_s = 0.073 the alpha time grows by ∼7 decades, and the difference increases even stronger at higher stickers fraction (Figure 11). These trends agree well with the theoretical predictions. The experimental data also show a stronger than exponential growth of the alpha time with sticker fraction as shown by an illustrative black dashed line through the cyan points in Figure 11. This is as predicted by the theory, a trend that has been experimentally observed for multiblock random copolymer melts and previously shown to be well captured by our same theory.[36]

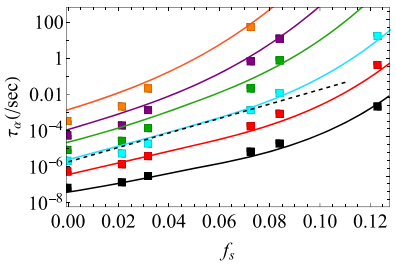

Figure 11. Alpha relaxation time (seconds) as a function of sticker fraction at various T/T_g ratios of 1.20, 1.16, 1.14, 1.12, 1.10, 1.08 (theory, black to orange curves) and 1.20, 1.16, 1.14, 1.12, 1.1, 1.08 (experiment, black to orange points) for PDMS-NCHO-COOH. The data points with τ_α > 10 s from experiments[28−33] are obtained from extrapolated VFT fits of the discrete experimental data. A linear fit through the first four cyan experimental points (dashed black line) is shown as an example to visually illustrate the supraexponential growth of the alpha time with respect to sticker fraction observed experimentally. The latter agrees well with theoretical predictions (coincident with the initial growth of cyan curve).

VI. APPLICATION TO PPG-BASED TELECHELIC MELTS: Shift in T_g

In this section we first present model calculations of how our theoretical predictions for the change of the glass transition temperature depend on introducing enhanced dynamic fluctuations of the stickers based on the new extension of the theory reported in section III. The theory is then applied to understand the behavior of the PPG-based weakly associating telechelic melts.

Change in T_g for Larger Sticker Fluctuation. Figure 12 plots the predicted change in nonsticker glass transition temperature for PDMS as a function of sticker fraction for three values of sticker fluctuation amplitude. The blue curve is the same as the blue solid curves in Figure 9 with the a priori predicted value of $r_L^{s\prime} = r_L^s$. The other two curves illustrate how larger sticker fluctuations ("looser and weaker bonds") change the theoretical results. If $r_L^{s\prime} = r_L^s + 0.33\Delta r_n$ (a displacement well below the nonsticker dynamic free energy barrier), then essentially all the constraints due to the presence of bonded stickers are predicted to disappear. This indicates a dynamic crossover to a regime of weak sticker associations which have little or no effect on the nonsticker alpha time. Importantly, such behavior can emerge *without* the need for the sticker alpha time becoming equal to its nonsticker analogue; i.e., the α and α^* relaxation events do *not* need to have an identical time scale. Qualitatively, we physically rationalize the predicted behavior by noting that $0.33\Delta r_n > a = 0.1d$ where a is the range of attractive interaction between stickers. Hence, this size of a sticker dynamic fluctuation is *larger* than the attraction range that defines a physical bond, and hence the predicted destruction of kinetic constraints on nonstickers due to sticker bonding seems physically intuitive. How fragility decreases as a

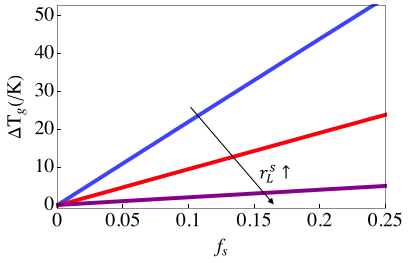

Figure 12. Theoretical predictions for the change of the nonsticker T_g due to the presence of stickers associated with enhanced sticker fluctuations as a function of sticker fraction for different values of $r_L^{s\prime} = r_L^s$ (blue), $r_L^s + 0.25\Delta r_n$ (red), and $r_L^s + 0.33\Delta r_n$ (purple) using the PDMS homopolymer mapping described in the main text (cf. Figure 5, blue line).

https://doi.org/10.1021/acs.macromol.2c00080
Macromolecules XXXX, XXX, XXX−XXX

function of sticker fraction for increasing degrees of sticker bond fluctuations is discussed in the SM.

Comparison of Theory and Experiment for PPG Systems. To predict the glass transition temperature changes for the weakly associating PPG telechelic melts, we adopt the same packing fraction to temperature mapping discussed in section III. However, the EOS state data appear to be unavailable for the PPG homopolymer. We thus use $A = 0.627$ and $B = 1353$ K parameters for PIB,[54] $\tau_0 = 10^{-12}$ s, and calibrate N_s to best reproduce the DP-dependent glass transition temperature of homopolymer PPG with non-associating chain ends. For the mapping used, we again adopt $f = a/DP$ where $a \sim 1.3$ based on $C_N \sim 6.8$ and $N_s \sim 5.2$ appropriate for PPG.[54] We note that using the specific mapping parameters for any other homopolymer does not change any of our results significantly since the adopted calibration step ensures we capture the correct DP-dependent homopolymer melt T_g.

The theoretical results for the shift of T_g are reported in Figure 13 for various end groups of the PPG telechelic melt.

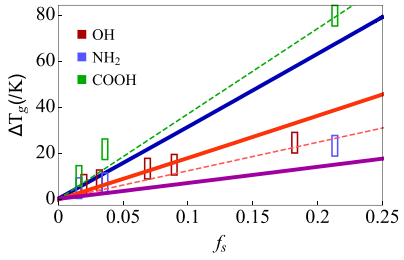

Figure 13. Change of T_g compared to the DP-dependent homopolymer melt as a function of sticker fraction for various sticker moieties attached to a PPG backbone. Theoretical predictions are given by the blue curve when stickers are localized at their respective a priori predicted localization lengths (r_L^s) corresponding to tight physical bonds. Red and purple curves correspond to theoretical results for larger sticker dynamic fluctuations of $r_L^{s\prime} = r_L^s + 0.25\Delta r_n$ and $r_L^s + 0.33\Delta r_n$, respectively. Experimental data are shown as the solid squares. A fit through the experimental COOH system points is indicated by the green dashed line, while those for NH_2 and OH are given in red (treating them as single set of data).

The blue solid line corresponds to when stickers fluctuate at the tight localization lengths that are a priori predicted. This result agrees well with our COOH-based experiments on the PPG telechelic melt. We believe that strong H-bonding between COOH groups is responsible for creating stronger bonding constraints and, hence, the larger growth in T_g.

The other two curves in Figure 13 are results when sticker fluctuations are larger than their respective localization lengths corresponding to weakened bonding constraints on the time scale of the activated relaxation of nonsticker segments. Specifically, we deduce that if stickers displace distances close to 1/4 to 1/3 of nonsticker hopping jump distance (a relatively small fractional distance), the theory captures well the experimentally observed smaller growth in T_g for PPG systems with NH_2 and OH end groups (theoretical red and purple curves, respectively). We note that when stickers are allowed to fluctuate with localization lengths close to a displacement of maximum force on the dynamic free energy of pure homopolymers (its inflection point in Figure 6B), i.e., $r_L^{s\prime} \sim r^*(f_s \to 0)$, dynamic caging constraints due to bonding are essentially entirely lost and the local barrier is nearly the same as that of the homopolymer (not plotted). In this case we see no change of T_g due to such dynamically weak associations. This limit corresponds to even weaker bonding constraints than appear to be appropriate for PPG with NH_2 or OH end groups in Figure 13.

VII. SUMMARY AND CONCLUSIONS

We have quantitatively tested predictions of our recently proposed[36] microscopic theory of how attractive forces and physical bonding in associating copolymer liquids affect segmental relaxation and the glass transition temperature against experimental data for telechelic PDMS- and PPG-based associating polymers. Theoretical results for the alpha relaxation time as a function of packing fraction are mapped to temperature space by using the polymer EOS that allows us to predict how the glass transition temperature changes for real associating materials. Remarkably, the large time scale separation between the nonsticker alpha relaxation and slower bond-breaking process for PDMS telechelic melts renders the systems oblivious to the specific type of attraction or even microphase separation for the question of the change of glass transition temperature as a function of sticker fraction. The data thus support the proposed physical idea that such systems behave as cross-linked networks on the time scale of the nonsticker alpha relaxation. More quantitatively, our microscopic *parameter free* theoretical predictions for the associating melts agree remarkably well with experiment, not only for how T_g changes with telechelic chain length but also for other important questions such as the sticker-induced supra-exponential growth of the alpha relaxation with sticker fraction that becomes stronger upon approaching T_g, and the perturbative or almost negligible changes of dynamic fragility with sticker fraction. These findings also support our hypothesis that changes of the nonsticker structural relaxation time are not affected (to leading order) by the precise transient network topology, at least for the copolymer architectures we have studied to date.

The theory has been extended in this work to lift the assumption of strong time scale separation between the nonsticker alpha time and the sticker bond breaking lifetime by allowing stickers to fluctuate within their predicted dynamic free energy to modestly larger length scales characteristic of the late beta or early alpha relaxation process of stickers while still retaining the same basic transient network like picture. This results in *dynamical* weakening of sticker bonding, which in turns reduces their effect on the activated relaxation of nonsticker activated relaxation. This advance provides an understanding of experimental observations of weakly associating PPG telechelic melts for −OH and $-NH_2$ end groups which exhibit much reduced T_g enhancements. On the other hand, for the strongly associating case of PPG-COOH, the theoretical prediction for the enhancement of T_g due to physical bond formation again agrees remarkably well with experiment.

Future joint theoretical−experimental work can explore the consequences of the presented level of understanding for the problem of material design and synthesis of associating polymers and polymers with dynamic covalent bonds. The present work also sets the stage to theoretically address other questions for melts of polymers with dynamic bonds, such as elastic reinforcement and change of flow viscosity where longer length/time-scale chain dynamics is strongly impacted by the nonperturbative changes of local segmental dynamics.

https://doi.org/10.1021/acs.macromol.2c00080
Macromolecules XXXX, XXX, XXX−XXX

■ ASSOCIATED CONTENT

Supporting Information

The Supporting Information is available free of charge at https://pubs.acs.org/doi/10.1021/acs.macromol.2c00080.

(i) A brief summary of the synthesis protocols of telechelic systems and (ii) details of the theory modeling of the reference homopolymer melt DP-dependent T_g and fragility (PDF)

■ AUTHOR INFORMATION

Corresponding Authors

Alexei P. Sokolov − *Department of Chemistry, University of Tennessee, Knoxville, Tennessee 37996, United States; Chemical Sciences Division, Oak Ridge National Laboratory, Oak Ridge, Tennessee 37831, United States;* orcid.org/0000-0002-8187-9445; Email: sokolov@utk.edu

Kenneth S. Schweizer − *Department of Materials Science & Engineering, Materials Research Laboratory, Department of Chemistry, and Department of Chemical & Biomolecular Engineering, University of Illinois at Urbana−Champaign, Urbana, Illinois 61801, United States*; Email: kschweiz@illinois.edu

Authors

Ashesh Ghosh − *Department of Chemical Engineering, Stanford University, Stanford, California 94305, United States; Materials Research Laboratory and Department of Chemistry, University of Illinois at Urbana−Champaign, Urbana, Illinois 61801, United States;* orcid.org/0000-0002-3312-6107

Subarna Samanta − *Department of Chemistry, University of Tennessee, Knoxville, Tennessee 37996, United States;* orcid.org/0000-0003-3386-5556

Sirui Ge − *Department of Material Science and Engineering, University of Tennessee, Knoxville, Tennessee 37996, United States;* orcid.org/0000-0002-4276-7838

Complete contact information is available at: https://pubs.acs.org/10.1021/acs.macromol.2c00080

Notes

The authors declare no competing financial interest.

■ ACKNOWLEDGMENTS

This work was supported by the U.S. Department of Energy, Office of Science, Basic Energy Sciences, Materials Sciences and Engineering Division. S.S. and S.G. acknowledge support for experimental part by NSF Polymer program under Award DMR-1904657.

■ REFERENCES

(1) Wang, C.; Wu, H.; Chen, Z.; McDowell, M. T.; Cui, Y.; Bao, Z. Self-Healing Chemistry Enables the Stable Operation of Silicon Microparticle Anodes for High-Energy Lithium-Ion Batteries. *Nat. Chem.* **2013**, *5* (12), 1042−1048.

(2) Olsen, B. D.; Kornfield, J. A.; Tirrell, D. A. Yielding Behavior in Injectable Hydrogels from Telechelic Proteins. *Macromolecules* **2010**, *43* (21), 9094−9099.

(3) Cao, P.-F.; Li, B.; Hong, T.; Townsend, J.; Qiang, Z.; Xing, K.; Vogiatzis, K. D.; Wang, Y.; Mays, J. W.; Sokolov, A. P.; Saito, T. Superstretchable, Self-Healing Polymeric Elastomers with Tunable Properties. *Adv. Funct. Mater.* **2018**, *28* (22), 1800741.

(4) Cordier, P.; Tournilhac, F.; Soulié-Ziakovic, C.; Leibler, L. Self-Healing and Thermoreversible Rubber from Supramolecular Assembly. *Nature* **2008**, *451* (7181), 977−980.

(5) Campanella, A.; Döhler, D.; Binder, W. H. Self-Healing in Supramolecular Polymers. *Macromol. Rapid Commun.* **2018**, *39* (17), 1700739.

(6) Huang, Y.-F.; Xu, J.-Z.; Xu, J.-Y.; Zhang, Z.-C.; Hsiao, B. S.; Xu, L.; Li, Z.-M. Self-Reinforced Polyethylene Blend for Artificial Joint Application. *J. Mater. Chem. B* **2014**, *2* (8), 971.

(7) Kim, M.; Chen, W. G.; Kang, J. W.; Glassman, M. J.; Ribbeck, K.; Olsen, B. D. Artificially Engineered Protein Hydrogels Adapted from the Nucleoporin Nsp1 for Selective Biomolecular Transport. *Adv. Mater.* **2015**, *27* (28), 4207−4212.

(8) Ma, M.; Guo, L.; Anderson, D. G.; Langer, R. Bio-Inspired Polymer Composite Actuator and Generator Driven by Water Gradients. *Science* **2013**, *339* (6116), 186−189.

(9) Wei, M.-H.; Li, B.; David, R. L. A.; Jones, S. C.; Sarohia, V.; Schmitigal, J. A.; Kornfield, J. A. Megasupramolecules for Safer, Cleaner Fuel by End Association of Long Telechelic Polymers. *Science* **2015**, *350* (6256), 72−75.

(10) Rosales, A. M.; Anseth, K. S. The Design of Reversible Hydrogels to Capture Extracellular Matrix Dynamics. *Nat. Rev. Mater.* **2016**, DOI: 10.1038/natrevmats.2015.12.

(11) Li, C.-H.; Wang, C.; Keplinger, C.; Zuo, J.-L.; Jin, L.; Sun, Y.; Zheng, P.; Cao, Y.; Lissel, F.; Linder, C.; You, X.-Z.; Bao, Z. A Highly Stretchable Autonomous Self-Healing Elastomer. *Nat. Chem.* **2016**, *8* (6), 618−624.

(12) Hagenau, A.; Suhre, M. H.; Scheibel, T. R. Nature as a Blueprint for Polymer Material Concepts: Protein Fiber-Reinforced Composites as Holdfasts of Mussels. *Prog. Polym. Sci.* **2014**, *39* (8), 1564−1583.

(13) Zhang, Z. P.; Rong, M. Z.; Zhang, M. Q. Polymer Engineering Based on Reversible Covalent Chemistry: A Promising Innovative Pathway towards New Materials and New Functionalities. *Prog. Polym. Sci.* **2018**, *80*, 39−93.

(14) Folmer, B. J. B.; Sijbesma, R. P.; Versteegen, R. M.; van der Rijt, J. A. J.; Meijer, E. W. Supramolecular Polymer Materials: Chain Extension of Telechelic Polymers Using a Reactive Hydrogen-Bonding Synthon. *Adv. Mater.* **2000**, *12* (12), 874−878.

(15) Filippidi, E.; Cristiani, T. R.; Eisenbach, C. D.; Waite, J. H.; Israelachvili, J. N.; Ahn, B. K.; Valentine, M. T. Toughening Elastomers Using Mussel-Inspired Iron-Catechol Complexes. *Science* **2017**, *358* (6362), 502−505.

(16) Albertazzi, L.; van der Zwaag, D.; Leenders, C. M. A.; Fitzner, R.; van der Hofstad, R. W.; Meijer, E. W. Probing Exchange Pathways in One-Dimensional Aggregates with Super-Resolution Microscopy. *Science* **2014**, *344* (6183), 491−495.

(17) Chen, Q.; Tudryn, G. J.; Colby, R. H. Ionomer Dynamics and the Sticky Rouse Model. *J. Rheol.* **2013**, *57* (5), 1441−1462.

(18) Holten-Andersen, N.; Harrington, M. J.; Birkedal, H.; Lee, B. P.; Messersmith, P. B.; Lee, K. Y. C.; Waite, J. H. PH-Induced Metal-Ligand Cross-Links Inspired by Mussel Yield Self-Healing Polymer Networks with Near-Covalent Elastic Moduli. *Proc. Natl. Acad. Sci. U. S. A.* **2011**, *108* (7), 2651−2655.

(19) Tang, S.; Wang, M.; Olsen, B. D. Anomalous Self-Diffusion and Sticky Rouse Dynamics in Associative Protein Hydrogels. *J. Am. Chem. Soc.* **2015**, *137* (11), 3946−3957.

(20) Zhang, Z.; Huang, C.; Weiss, R. A.; Chen, Q. Association Energy in Strongly Associative Polymers. *J. Rheol.* **2017**, *61* (6), 1199−1207.

(21) Leibler, L.; Rubinstein, M.; Colby, R. H. Dynamics of Reversible Networks. *Macromolecules* **1991**, *24* (16), 4701−4707.

(22) Semenov, A. N.; Rubinstein, M. Thermoreversible Gelation in Solutions of Associative Polymers. 1. Statics. *Macromolecules* **1998**, *31* (4), 1373−1385.

(23) Rubinstein, M.; Semenov, A. N. Thermoreversible Gelation in Solutions of Associating Polymers. 2. Linear Dynamics. *Macromolecules* **1998**, *31* (4), 1386−1397.

(24) Rubinstein, M.; Semenov, A. N. Dynamics of Entangled Solutions of Associating Polymers. *Macromolecules* **2001**, *34* (4), 1058−1068.
(25) van Ruymbeke, E.; Vlassopoulos, D.; Mierzwa, M.; Pakula, T.; Charalabidis, D.; Pitsikalis, M.; Hadjichristidis, N. Rheology and Structure of Entangled Telechelic Linear and Star Polyisoprene Melts. *Macromolecules* **2010**, *43* (9), 4401−4411.
(26) Ahmadi, M.; Hawke, L. G. D.; Goldansaz, H.; van Ruymbeke, E. Dynamics of Entangled Linear Supramolecular Chains with Sticky Side Groups: Influence of Hindered Fluctuations. *Macromolecules* **2015**, *48* (19), 7300−7310.
(27) Cates, M. E. Reptation of Living Polymers: Dynamics of Entangled Polymers in the Presence of Reversible Chain-Scission Reactions. *Macromolecules* **1987**, *20* (9), 2289−2296.
(28) Ge, S.; Tress, M.; Xing, K.; Cao, P.-F.; Saito, T.; Sokolov, A. P. Viscoelasticity in Associating Oligomers and Polymers: Experimental Test of the Bond Lifetime Renormalization Model. *Soft Matter* **2020**, *16* (2), 390−401.
(29) Xing, K.; Tress, M.; Cao, P.-F.; Fan, F.; Cheng, S.; Saito, T.; Sokolov, A. P. The Role of Chain-End Association Lifetime in Segmental and Chain Dynamics of Telechelic Polymers. *Macromolecules* **2018**, *51* (21), 8561−8573.
(30) Xing, K.; Chatterjee, S.; Saito, T.; Gainaru, C.; Sokolov, A. P. Impact of Hydrogen Bonding on Dynamics of Hydroxyl-Terminated Polydimethylsiloxane. *Macromolecules* **2016**, *49* (8), 3138−3147.
(31) Tress, M.; Xing, K.; Ge, S.; Cao, P.; Saito, T.; Sokolov, A. What Dielectric Spectroscopy Can Tell Us about Supramolecular Networks. *Eur. Phys. J. E* **2019**, DOI: 10.1140/epje/i2019-11897-4.
(32) Xing, K.; Tress, M.; Cao, P.; Cheng, S.; Saito, T.; Novikov, V. N.; Sokolov, A. P. Hydrogen-Bond Strength Changes Network Dynamics in Associating Telechelic PDMS. *Soft Matter* **2018**, *14* (7), 1235−1246.
(33) Tress, M.; Ge, S.; Xing, K.; Cao, P.-F.; Saito, T.; Genix, A.-C.; Sokolov, A. P. Turning Rubber into a Glass: Mechanical Reinforcement by Microphase Separation. *ACS Macro Lett.* **2021**, *10* (2), 197−202.
(34) Mordvinkin, A.; Döhler, D.; Binder, W. H.; Colby, R. H.; Saalwächter, K. Rheology, Sticky Chain, and Sticker Dynamics of Supramolecular Elastomers Based on Cluster-Forming Telechelic Linear and Star Polymers. *Macromolecules* **2021**, *54* (11), 5065−5076.
(35) Samanta, S.; Kim, S.; Saito, T.; Sokolov, A. P. Polymers with Dynamic Bonds: Adaptive Functional Materials for a Sustainable Future. *J. Phys. Chem. B* **2021**, *125* (33), 9389−9401.
(36) Ghosh, A.; Schweizer, K. S. Microscopic Theory of the Effect of Caging and Physical Bonding on Segmental Relaxation in Associating Copolymer Liquids. *Macromolecules* **2020**, *53* (11), 4366−4380.
(37) Ghosh, A.; Schweizer, K. S. Physical Bond Breaking in Associating Copolymer Liquids. *ACS Macro Lett.* **2021**, *10* (1), 122−128.
(38) Ge, S.; Samanta, S.; Tress, M.; Li, B.; Xing, K.; Dieudonné-George, P.; Genix, A.-C.; Cao, P.-F.; Dadmun, M.; Sokolov, A. P. Critical Role of the Interfacial Layer in Associating Polymers with Microphase Separation. *Macromolecules* **2021**, *54* (9), 4246−4256.
(39) Gold, B. J.; Hövelmann, C. H.; Lühmann, N.; Székely, N. K.; Pyckhout-Hintzen, W.; Wischnewski, A.; Richter, D. Importance of Compact Random Walks for the Rheology of Transient Networks. *ACS Macro Lett.* **2017**, *6* (2), 73−77.
(40) Shabbir, A.; Javakhishvili, I.; Cerveny, S.; Hvilsted, S.; Skov, A. L.; Hassager, O.; Alvarez, N. J. Linear Viscoelastic and Dielectric Relaxation Response of Unentangled UPy-Based Supramolecular Networks. *Macromolecules* **2016**, *49* (10), 3899−3910.
(41) Wu, S.; Liu, S.; Zhang, Z.; Chen, Q. Dynamics of Telechelic Ionomers with Distribution of Number of Ionic Stickers at Chain Ends. *Macromolecules* **2019**, *52* (6), 2265−2276.
(42) Mordvinkin, A.; Suckow, M.; Böhme, F.; Colby, R. H.; Creton, C.; Saalwächter, K. Hierarchical Sticker and Sticky Chain Dynamics in Self-Healing Butyl Rubber Ionomers. *Macromolecules* **2019**, *52* (11), 4169−4184.
(43) Schweizer, K. S.; Curro, J. G. Integral Equation Theory of Polymer Melts: Intramolecular Structure, Local Order, and the Correlation Hole. *Macromolecules* **1988**, *21* (10), 3070−3081.
(44) Schweizer, K. S.; Curro, J. G. Integral Equation Theories of the Structure, Thermodynamics, and Phase Transitions of Polymer Fluids. *Adv. Chem. Phys.* **2007**, *98*, 1−142.
(45) Kolbet, K. A.; Schweizer, K. S. Real Space Structure of Associating Polymer Melts. *Macromolecules* **2000**, *33* (4), 1443−1458.
(46) Sung, B. J.; Yethiraj, A. Integral Equation Theory of Random Copolymer Melts: Self-Consistent Treatment of Intramolecular and Intermolecular Correlations. *J. Chem. Phys.* **2005**, *122* (23), 234904.
(47) Hansen, J.-P.; Mcdonald, I. R. *Theory of Simple Liquids*; Jordan Hill Elsevier Science: 2014.
(48) Mirigian, S.; Schweizer, K. S. Elastically Cooperative Activated Barrier Hopping Theory of Relaxation in Viscous Fluids. I. General Formulation and Application to Hard Sphere Fluids. *J. Chem. Phys.* **2014**, *140* (19), 194506.
(49) Mirigian, S.; Schweizer, K. S. Elastically Cooperative Activated Barrier Hopping Theory of Relaxation in Viscous Fluids. II. Thermal Liquids. *J. Chem. Phys.* **2014**, *140* (19), 194507.
(50) Viehman, D. C.; Schweizer, K. S. Theory of Gelation, Vitrification, and Activated Barrier Hopping in Mixtures of Hard and Sticky Spheres. *J. Chem. Phys.* **2008**, *128* (8), 084509.
(51) Dell, Z. E.; Schweizer, K. S. Microscopic Theory for the Role of Attractive Forces in the Dynamics of Supercooled Liquids. *Phys. Rev. Lett.* **2015**, DOI: 10.1103/PhysRevLett.115.205702.
(52) Ghosh, A.; Schweizer, K. S. Microscopic Theory of the Influence of Strong Attractive Forces on the Activated Dynamics of Dense Glass and Gel Forming Fluids. *J. Chem. Phys.* **2019**, *151* (24), 244502.
(53) Here the logic is Δr is a function of ϕ_{eff} and stickers are allowed to fluctuate to a displacement equivalent to 1/4 or 1/3 of the distance required for the full hop (the α^* relaxation event). So, our choices maintain a fixed ratio of the jump length scale and adjusts (jump length)/d per the value of ϕ (maps to temperature). If one chooses to implement this idea assuming, e.g., $r_L^{s\prime} = r_L^s, r_L^s + 0.10d$, or $r_L^s + 0.20d$, this does not change the results qualitatively.
(54) Mirigian, S.; Schweizer, K. S. Dynamical Theory of Segmental Relaxation and Emergent Elasticity in Supercooled Polymer Melts. *Macromolecules* **2015**, *48* (6), 1901−1913.
(55) Hintermeyer, J.; Herrmann, A.; Kahlau, R.; Goiceanu, C.; Rössler, E. A. Molecular Weight Dependence of Glassy Dynamics in Linear Polymers Revisited. *Macromolecules* **2008**, *41* (23), 9335−9344.
(56) Fox, T. G.; Loshaek, S. Influence of Molecular Weight and Degree of Crosslinking on the Specific Volume and Glass Temperature of Polymers. *J. Polym. Sci.* **1955**, *15* (80), 371−390.
(57) Fox, T. G.; Flory, P. J. Second-Order Transition Temperatures and Related Properties of Polystyrene. I. Influence of Molecular Weight. *J. Appl. Phys.* **1950**, *21* (6), 581−591.
(58) To be more accurate, because the temperatures calculated as xT_g can be any T between the experimentally measured points, the data were interpolated between the nearest points using the VFT expression. In this case the error bar is not very large. The VFT fit parameters can be found in references mentioned in the main text.

https://doi.org/10.1021/acs.macromol.2c00080
Macromolecules XXXX, XXX, XXX−XXX